



Commissioning and operation of the cryostat for 3W1 SC wiggler

Miao-Fu Xu^{1,2,3} · Xiang-Zhen Zhang^{1,2,3} · Rui Ye^{1,2,3} · Jin-Can Wang¹ · Xiao-Juan Bian^{1,2} · Yao Gao^{1,2} · Min-Xian Li^{1,2} · Fu-San Chen^{1,2,4} · Xiao-Chen Yang^{1,2,3} · Rui Ge^{1,2,3,4}

Received: 26 November 2022 / Revised: 15 March 2023 / Accepted: 28 March 2023 / Published online: 27 June 2023

© The Author(s), under exclusive licence to China Science Publishing & Media Ltd. (Science Press), Shanghai Institute of Applied Physics, the Chinese Academy of Sciences, Chinese Nuclear Society 2023

Abstract

A 3W1 superconducting wiggler (SCW) with the pole gap of 68 mm was successfully tested and installed in a BEPC II storage ring in November, 2019. The goal of zero liquid helium consumption was achieved, and the cryogenic system exhibited a 12% residual cooling capacity (approximately 0.69 W @4.2 K). The 3W1-SCW was set to operate at 2.49 T and has been operating for more than seven months. Three instances of magnet quenching occurred during the normal operation. The evaporated helium gas can be recycled to the helium gas recycling system when the pressure in the helium tank is higher than the parameter value (the setpoint of the pressure value is 1.2 bara). The cryogenic system can be recovered within 4 h if sufficient liquid helium is available to inject into the cryostat.

Keywords Cryostat · Commissioning · SC wiggler · Synchrotron radiation

1 Introduction

The spectral characteristics of synchrotron radiation (SR) from a bending magnet are determined by two parameters: electron energy E and magnetic field B . To improve SR quality, at the Beijing Electron Positron Collider Upgrade Project (BEPC II), increasing the electron energy is not easy because the corresponding storage ring has been operating for many years and cannot work at high electron energies. However, there is an inexpensive and simple alternative method to achieve this: Superconducting (SC) insertion devices such

as SC wigglers (SCWs) are often used as the first choice to replace old permanent magnets [1].

The 3W1-SCW was scheduled to operate at 2.49 T, which is feasible for beam-load work. A cryogenic system for SC magnets should be based on the principles of reliability, stability, and safety for beam-load work and experiments. Further, the cryostat design should meet the long-term machine operation without the requirement for liquid helium refilling; more specifically, the cryogenic system should have sufficient residual cooling capacity for a prolonged lifecycle (1–1.5 a) under zero helium consumption conditions [2].

Owing to the heat conductivity between the upstream and downstream parts of the beam tube, the actual heat load of the helium bath exceeded the expected value after the insertion device was installed in the storage ring. The total dynamic thermal load from the stored beam could not be accurately calculated and estimated. The measured contribution to the total heat load from the stored beam in MAX II was 0.86 W instead of the predicted 0.17 W, and the contribution to the beam-induced heating from the image current was 0.59 W, approximately 10 times larger than expected from calculations [3]. The helium evaporation was significantly higher than expected after two SCWs were installed in the Diamond Light Source (DLS) storage ring in March, 2009, and liquid helium must be refilled more frequently to maintain the respective cryogenic system. This not only increases the cost, but also limits the operating beam current

✉ Rui Ge
gerui@ihep.ac.cn
Miao-Fu Xu
xumf@ihep.ac.cn

¹ Institute of High Energy Physics, Chinese Academy of Sciences, Beijing 100049, China

² Key Laboratory of Particle Acceleration Physics and Technology, Chinese Academy of Sciences, Beijing 100049, China

³ Center for Superconducting RF and Cryogenics, Institute of High Energy Physics, Beijing 100049, China

⁴ University of Chinese Academy of Sciences, Beijing 100049, China

[4]. Accordingly, a copper liner was installed in the vacuum chamber to intercept dynamic thermal loads generated by image current, electron clouds, and SR [2, 5, 6].

A 3W1 32-pole SCW for a high-energy photon source test facility was designed by the Institute of High Energy Physics (IHEP) and fabricated in Vacree (Hefei, Anhui). It passed acceptance tests and a two-month reliability experiment at the manufacturing site in May, 2019, in which various modes of wiggler operation, including the functionality of the cryogenic and controlling systems, were checked and the magnetic field characteristics were measured [7–9]. In particular, the magnet's first and second field integrals were evaluated using a tension line measuring system, and the results showed that operation of the 3W1-SCW does not affect the working reliability of the storage ring [10]. The test commission must be completed before the cryostat is installed in the storage ring of BEPC II, including analyses of the cryogenic system, magnetic field, quench protection system (QPS), power supply system, control system, and alignment. Figure 1 shows the 3W1-SCW installed in the storage ring of BEPC II.

2 Magnetic field test

The performances of the cryogenic and magnet systems were retested after the device was transported to the IHEP site. It took one month to build a test site for the 3W1 SCW in Hall #5 at the IHEP, including systems to examine the liquid helium injection, helium gas recovery, and magnetic field. In particular, the magnetic field was remeasured using the Hall sensor system and tension line system to ensure the corresponding requirements were met and that the magnet was ready for operation (Fig. 2). Magnetic field measurements of the 3W1-SCW were carried out in Cartesian coordinates, which have designations x , y , and z : the z -axis coincides with



Fig. 1 (Color online) 2.6-T 32-pole superconducting wiggler (SCW) for high-energy photon source test facility

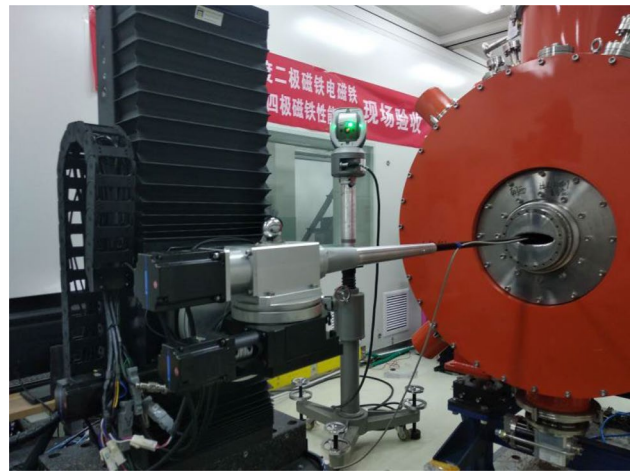


Fig. 2 (Color online) Hall sensor system used to measure the magnetic field

the longitudinal axis of the beam tube, while x and y are the horizontal and vertical directions, respectively. Equation (1) describes the SCW field [11, 12]. The distribution of B_y at different positions along the cross section of the beam tube is presented in Fig. 3.

$$B_{y0} = \hat{B} \cos\left(\frac{2\pi}{\lambda_{ID}}z\right), \quad (1)$$

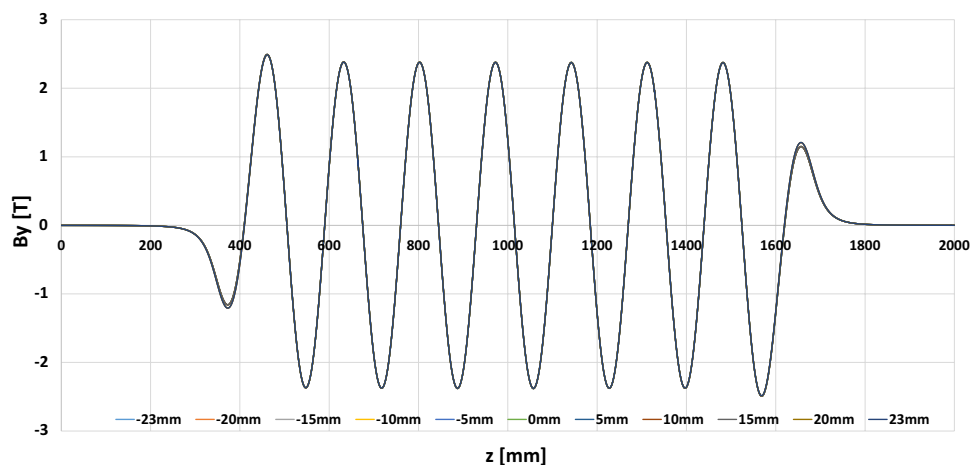
where B_{y0} is the wiggler magnetic field when $y=0$ mm, \hat{B} is the peak field intensity, and λ_{ID} is the magnetic field period length of the insertion element. According to the test results, the magnetic field meets our design requirements and the cryogenic system runs stably, consistent with the factory acceptance test results; therefore, the designed SCW is suitable for BEPC-II tunnel installation.

3 Quench protection system

A QPS is required for the 3W1 SCW magnet that not only reliably protects the SC elements (including 34 SC coils and six binary SC current leads, among others) from the damage caused by the release of heat when the magnet quenches [13, 14], but also supplies sufficient quench-related information for users to perform quench analysis. Accordingly, an active equipment was designed and developed for the QPS, constituting three cooperative subsystems: a digital quench detector (DQD), quench protection assembly (QPA), and software implementation.

The magnet quenching signal can be detected by monitoring the differential tap voltages and the time derivative of the excitation current in real time. These electrical signals are converted into digital signals, which are then analyzed using

Fig. 3 Distribution of B_y at different positions along the cross section of beam tube



DQD based on a digital signal processing (DSP) algorithm. Upon detection of a quench or other significant failures, the DQD sends a quench trigger link to both hardware and software elements to activate the magnet protection codes and data recording sequences. Multiple quench threshold values can be set for special-purpose triggers, and the channel configuration is programmable. In particular, the DQD system is constantly being improved because of heartbeat signals: the actions following the loss of heartbeat signals are similar to those of magnet quenching [15].

The power supply integrated with the QPA provides the user with direct control over the power of the magnet. When

a quench signal is detected, the power supply is immediately turned off and the energy extraction dump resistor is activated (Fig. 4).

The software implementation included two elements: data acquisition and real-time control [16]. During normal operation, voltage taps and other channels were continuously monitored and recorded at a slow rate of up to one sample per second. However, when a quench occurs, such data are collected at a high rate.

The QPS for the 3W1-SCW successfully worked for 3 quenches during the operation with beams and proved capable of actively limiting the energy released during a

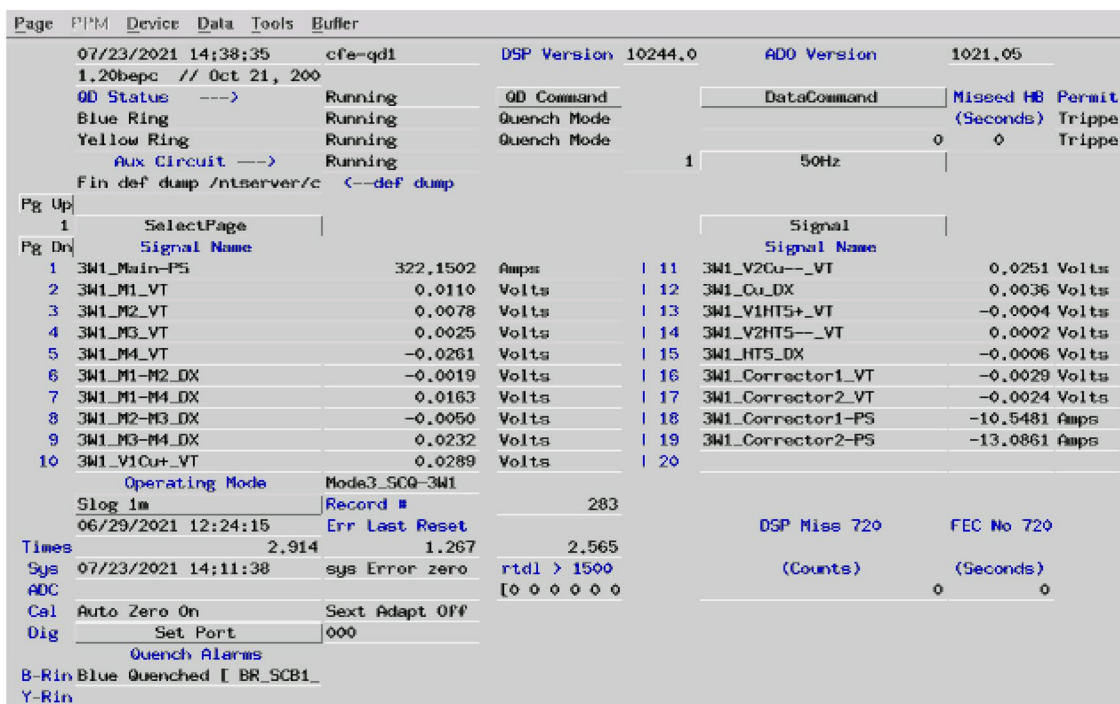


Fig. 4 Main control panel for quench protection assembly (QPA)

quench. Moreover, the flexibility of the system allowed a slight adjustment of the quench detection parameters.

4 Power supply control system

Control of the power supply was tested to ensure that the field of the wiggler was adjustable during operation. The cryogenic system should be ready before the magnet is powered up. The key parameters of the cryogenic system, including the level of liquid helium, pressure of the helium tank or temperature of the SC magnet, vacuum of the cryostat, and temperature of the thermal shields, are interlocked with the power supply control system to avoid damage to the SC magnet. Figure 5 displays the desired and actual current values for the key parameters of the



Fig. 5 Desired and actual current values of the key parameters of cryogenic system

cryogenic system. The desired current of the magnet under normal operation was confirmed through several commissioning and magnetic field tests.

The power-supply system can be operated when the signal of the cryogenic system set is ready and received. The power-on procedure involves the following steps:

The first step is to change the target current of the main power supply to 100 A and then start powering the magnet to the desired current value. The up- and down-current velocities were confirmed according to the offline test results, which also met the storage ring operation requirements. These can be compiled into a control program that cannot be changed by operators to avoid misoperation.

The second step is to change the target current of the main power supply to 200 A after a 20-min interval, and then start the power on the magnet to the desired current value.

The third step is to change the target current of the main power supply to 300 A after a 20-min interval, and then start powering the magnet to the desired current value.

The fourth step is to change the main power supply's target current to 320 A after a 20-min interval, and then start powering the magnet to the desired current value.

The fifth step is to change the target current of the west-correcting coil power supply to -10.99 A after a 10-min interval, and then start powering the magnet to the desired current value.

The sixth step is to change the target current of the east-correcting coil power supply to -13.20 A after a 10-min interval, and then start powering the magnet to the desired current value. Figure 6 shows the power control system interface.

The purpose of the intervals in steps 2–4 is to cool the SC magnet completely, particularly the Joule heat of the joint.

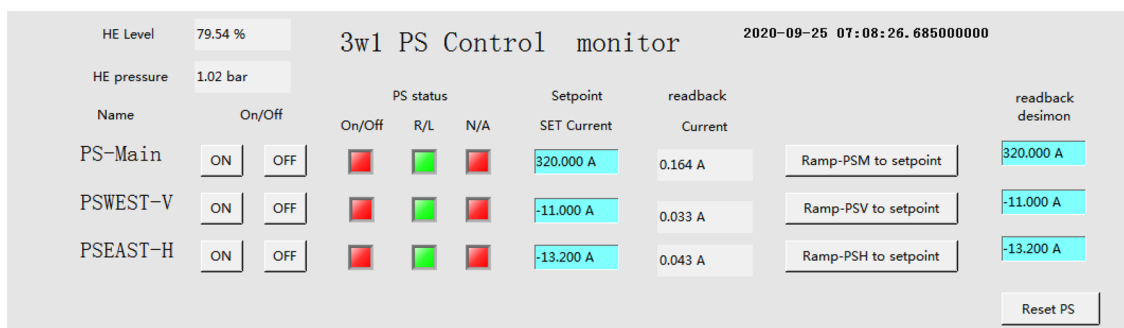


Fig. 6 Power control system interface

5 Storage ring installation

In November, 2019, the 3W1-SCW was installed in the storage ring of BEPC II to replace the old permanent wiggler after all preparatory work had been completed, including the magnetic field retest, QPS test, and corresponding transportation scheme, among others. The narrow width and limited height of the existing BEPC II tunnel bring more challenges to the transportation and installation of the 3W1-SCW (see Fig. 7a). The only choice of transportation scheme was the traditional roller transportation method, as depicted in Fig. 7b.

The location of the cryostat was adjusted using special tools based on the collimation results. New upstream and downstream vacuum chambers were installed after the 3W1-SCW cryostat was fixed (Fig. 8a, b). In particular, repeated optical surveying should be performed to ensure alignment of the magnet to the beam pipe within 0.1 mm.

The vibration of the beam line should be reduced as much as possible, which will affect the beam dynamics.

Cryocoolers are the main source of vibration, with the working frequency of 1 Hz. Special welding bellows were used to isolate vibrations from the cryostat and other devices on the beamline. The maximum amplitude of the cryostat was measured using a vibration monitor. The six measurement points are marked in Fig. 9 and the results are listed in Table 1.

The test results showed that the maximum amplitude of the vacuum house of the cryostat was much smaller than that of the cryocooler itself, indicating that the damping structures were very useful. The maximum amplitude of the cryostat, except the cryocooler, is 17 μm , which satisfies the requirement of the BEPC II storage ring operation.

6 Control system

The control system for the 3W1-SCW was based on embedded EPICS and integrated into the BEPC II center control system in November, 2019. Figure 10 presents the structure of the control system. The control system is an independent

Fig. 7 (Color online) Transport process of 3W1-SCW cryostat in the tunnel of the Beijing Electron Positron Collider Upgrade Project (BEPC II). **a** 3W1-SCW cryostat transportation in the BEPC II tunnel; **b** Diagram of specific transport program

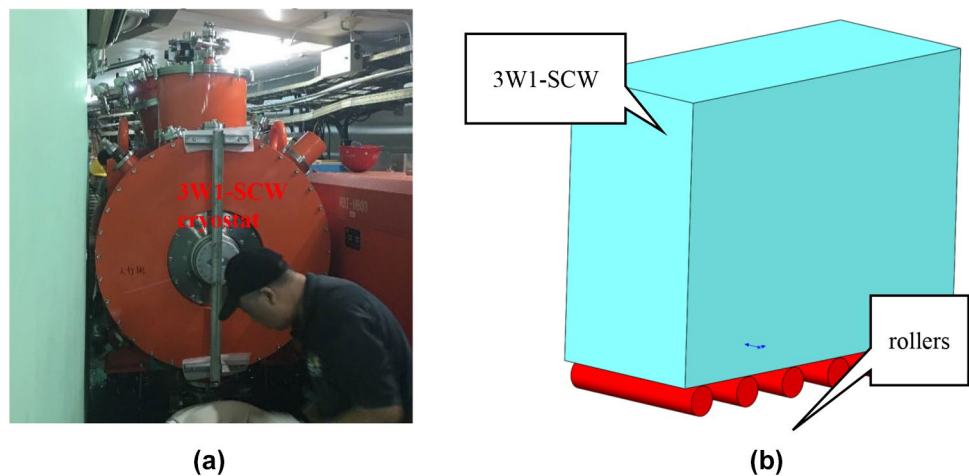
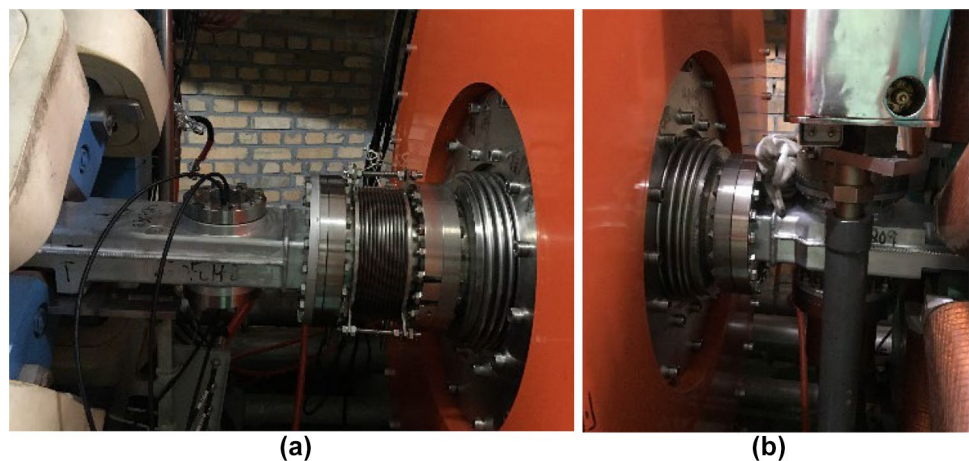


Fig. 8 (Color online) Photos of new upstream and downstream vacuum chamber. **a** Upstream vacuum chamber; **b** Downstream vacuum chamber



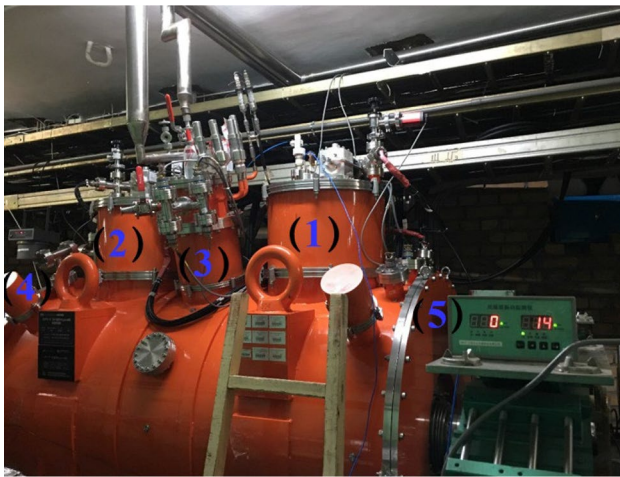


Fig. 9 (Color online) Vibration measuring points on the cryostat

Table 1 Test results of vibration measurement

Number	Measuring point	Maximum amplitude
1	Cryocooler tower 1	14 μm
2	Cryocooler tower 2	14 μm
3	Service tower	13 μm
4	Side flange 2	17 μm
5	Side flange 1	16 μm

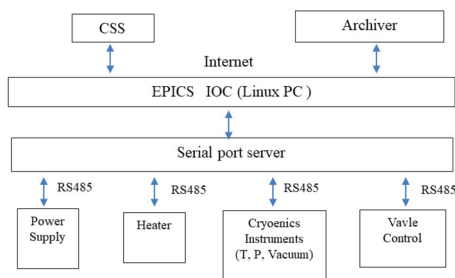


Fig. 10 Control algorithm of 3W1-SCW

system that can be used to perform signal conditioning for the quench detector, power supply input/output control, liquid helium level and pressure alarm of the helium vessel, electropneumatic valve opening/closing control, and the temperature of the SC magnet.

The control system for 3W1-SCW is also a distributed control system that provides remote and local operations. It comprises two major parts: a remote monitoring computer in the central control room of BEPC II and a local control computer in the area near the cryostat. Communication between computers occurs via the internet. The control authority of the local control computer was higher than that of the remote

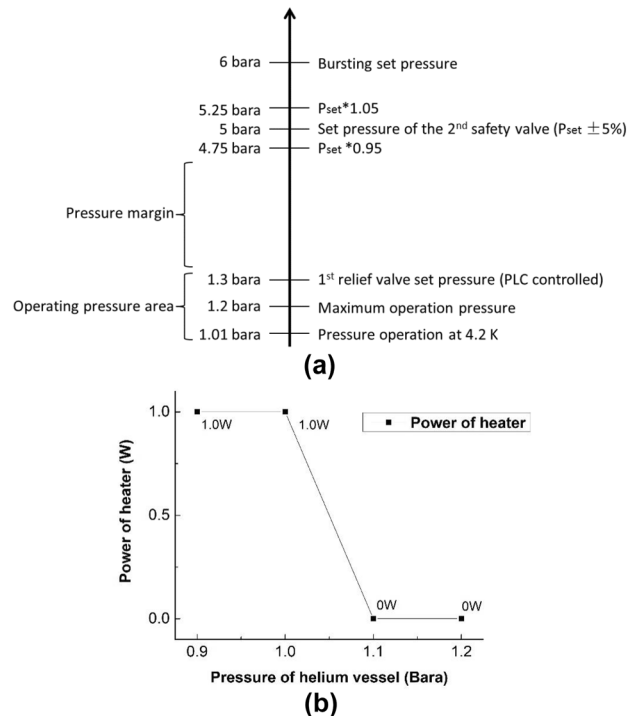


Fig. 11 Control of internal pressure in cryostat. a Operating pressure scale of cryostat; b Algorithm for power control of heater

monitoring computer. All data were automatically saved in the data server, which worked independently and was powered by an uninterruptible power supply.

The control system controls one main power supply and two correctional power supplies that modify the electron beam orbit and compensate for the integral field strength. The input/output speed of the magnetic current significantly affected the dynamic heat load and magnet quenching times. The dynamic heat load includes the Joule heat of the connectors and eddy current heat of the thermal shield for the beam tube. The operation input/output speeds of one main power supply and two correctional power supplies were identified after pre-commissioning.

Pressure is a sensitive and rapid indicator of heat-load changes. To be conservative and maintain a sufficient working pressure margin, a PLC-controlled valve was installed as the first relief valve, and the released helium gas was automatically stored in a helium gas bag. Parallel to the passive safety valve, the PLC-controlled valve opens at the absolute pressure of 1.2 bara, which is less than the design pressure of the cryostat. The pressure scale for operation of the cryostat safety device is shown in Fig. 11a.

The control system also has a self-checking function during normal operation. The necessary prerequisites for the ready signals were the level of liquid helium (> 95%), pressure of the helium vessel (< 1.2 bara), and temperature of the magnet (< 4.4 K). An electric heater was installed inside the

helium vessel, and its power was interlocked with the internal pressure. A control algorithm for the power control of the heater was formulated to solve the feedback control delay and reduce the helium pressure fluctuation. Figure 11b illustrates the control algorithm for power control of the heater. The alarm signals are listed in Table 2.

7 Cryogenic plumbing

Cryogenic plumbing involves two separate circuits made of stainless-steel tubes: helium transportation and helium gas recovery. Liquid helium was injected using a special cryogenic pipeline from a mobile helium dewar to a helium vessel (Fig. 12a). A cryogenic hand valve installed in the cryogenic pipeline was used to adjust the flow of liquid helium to control the rate of cooling of the cold mass during the cooling period. Owing to radiation in the tunnel, the injection pipeline of the cryostat leads to SR hall #10, which is near the cryostat installation site. The liquid helium of the mobile helium dewar can be injected into the helium tank using a special cryogenic pipeline when the level of liquid helium in the tank is below a set point. This method can significantly reduce the system recovery time when an SC magnet is quenched.

A helium gas recovery circuit was adopted in all the three cases. The first case involved cooling of the cryogenic pipeline. A small amount of air will be trapped inside the cryogenic pipeline after connection from the mobile helium dewar to the cryostat; therefore, the valves of CV02 and EPV04 should be closed, while CV03 should be open at the beginning of liquid helium injection to displace the air inside the pipe and cool the warm pipeline slowly. As a result, all the impure helium gas was reclaimed without waste. The second case involved

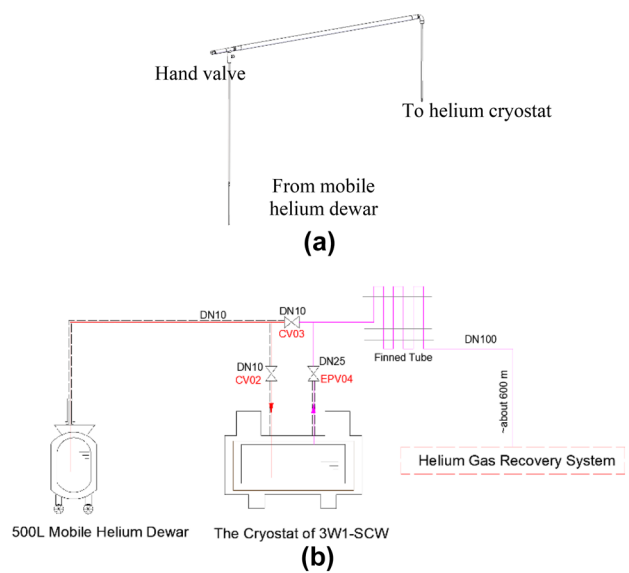


Fig. 12 Helium cryogenic system pipes. **a** Special cryogenic pipeline from mobile helium dewar to helium vessel; **b** Process diagram of cryogenic plumbing

the injection of liquid helium. Accordingly, the valve of CV03 should be closed and the valves of CV02 and EPV04 should be open; all pure helium gas will also be reclaimed. The third case involves pressure relief for any reason, particularly when the magnet is quenched or the insulation vacuum breaks down. The automatic pressure-relief valve, EPV04, can release the pressure of the helium vessel when the pressure exceeds the set value. A diagram depicting the process of cryogenic plumbing is presented in Fig. 12b. The distance from the cryostat to the helium gas bag was approximately 320 m, and a DN100 stainless-steel tube was used to reduce flow resistance.

Table 2 Alarm signals of control system

Number	Name	Label	Alarm value
1	Insulation vacuum	PI1000	$> 1 \times 10^{-3}$ Pa
2	Level of liquid helium	LIS101	$< 90\%$
3	Pressure of helium vessel	PI5101	> 1.20 bara
4	Temperature of magnets	TI5102	> 4.4 K
5	Temperature of 50 K stage of cryocooler (1#)	TI1202	> 50 K
6	Temperature of 4.2 K stage of cryocooler (1#)	TI1101	> 5 K
7	Temperature of 50 K stage of cryocooler (2#)	TI2202	> 50 K
8	Temperature of 4.2 K stage of cryocooler (2#)	TI2101	> 5 K
9	Temperature of 50 K stage of cryocooler (3#)	TI3202	> 50 K
10	Temperature of 4.2 K stage of cryocooler (3#)	TI3101	> 5 K
11	Temperature of 50 K stage of cryocooler (4#)	TI4202	> 50 K
12	Temperature of 4.2 K stage of cryocooler (4#)	TI4101	> 5 K
13	Temperature of thermal shields (vacuum chamber-west side)	TI5301	> 50 K
14	Temperature of thermal shields (vacuum chamber-east side)	TI5304	> 50 K

8 Commissioning

8.1 Cryogenic system and beam vacuum

In October 2019, the 3W1-SCW passed helium spectrometry leak detection and cryogenic pipeline pressure tests after installation was completed. Various modes of the wiggler operation, including the functions of the cryogenic and control systems, were checked and tested. The BEPC II storage ring operates in two modes: collision and SR. There is only two months for the SR mode in a cycle of operation, which is sufficient time for precooling only by cryocoolers. It took approximately six days to cool the cold mass using only cryocoolers from room temperature to the working temperature, and one day for liquid helium injection and thermal balance. The pressure of the helium tank will be less than the atmospheric pressure during the cooling period caused by helium gas contraction, which is not allowed and may damage the seal structure. Therefore, it is necessary to maintain the pressure stability by high purity helium gas which use a pressure reducing regulator to safely discharged from cylinder. After the control system pass the self-checking function, we attempted to increase the magnet current to 320 A at the speed of 0.2 A/s without an electron beam three times at the beginning of commissioning to ensure that the 3W1-SCW is ready for operation with the beam.

Because of the gas evolution of the newly installed upstream and downstream vacuum chambers, the vacuum is insufficient, resulting in a less efficient injection rate and short beam lifetime. Thus, the beam commissioning was delayed by four days to deal with the vacuum problem and

optimize the injection process to reduce the beam loss. A baking method was employed to increase the vacuum in the beam chamber.

The residual cooling capacity of cryogenic system is 0.69 W @4.2 K without the beam and 0.65 W @4.2 K with 250 mA electron beam intensity, hence the dynamic heat load which induced by beam is 0.04 W @4.18 K. However, the orbit of the beam should be adjusted according to the beam dynamics to meet the requirements of the new beam-line of the BEPC II SR facility. The cryostat temperature field is depicted in Fig. 13.

8.2 Beam position and spectral characteristic tests

The 3W1-SCW was ready to produce SR for users on November 14 and the control system was in working order. The cryogenic system can be operated as steadily as before. The SCW can affect beam dynamics including orbit change, beam lifetime, and beam performance; therefore, the beam orbit, initial phase, and bunch shape should be optimized to meet the requirements of SR [13, 17, 18]. The copper liner, which is installed between the beam tube and the 4.2 K vacuum chamber, acts as a thermal shield screen, protecting the vacuum chamber from heat induced by an electron beam in an accelerator.

We evaluated the beam power dissipation on the beam pipe in the cryostat with varying beam horizontal offset of 0, -12, and 12 mm, using the code CST. The primary parameters of the beams and beam pipes are listed in Table 3. Table 4 presents the results of the beam power dissipation with different horizontal offsets.

A series of beam-position tests were performed, in which the beam position exhibited a strong dependence on the

Fig. 13 (Color online) Graphical user interface (GUI) for 3W1-SCW control

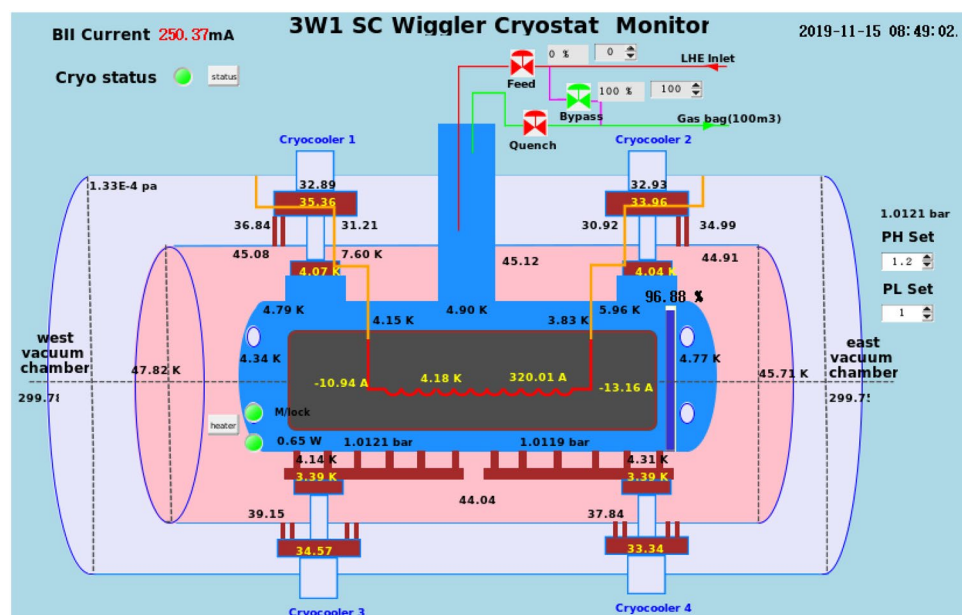


Table 3 Main parameters of the beam and the beam pipe

Parameter	Value
RMS bunch length (cm)	1.5
Total beam intensity (mA)	910
Number of bunches	93
Circumference (m)	237.53
Vacuum chamber (vertical) (mm)	39
Vacuum chamber (horizontal) (mm)	108
Length of the beam pipe (m)	1.965
Material of the beam pipe	Stainless steel with 0.1 mm of copper coating on the inner surface

Table 4 Loss factor and beam power dissipation with different horizontal offset

Horizontal offset (mm)	RMS beam length = 1.5 cm			
	Power loss on cryogenic part of beam pipe (W)	Power loss on warm chamber on both sides (W)	Loss factor (V/pC)	Total beam power loss (W)
0	13.4	57.4	2.6E-2	183
-12	14.1	50.7	1.5E-2	106
12	15.6	94.0	7.4E-2	522

dynamic thermal load of the cryogenic system, which is consistent with the experimental conclusion of the 25 + 2 pole wiggler of the Canadian Light Source [19]. Device operations and modifications to the storage ring would affect the dynamic heat load on the cryogenic system and the quality of SR. The highest dynamic heat load measured was 0.54 W @4.2 K when the orbit of the beam in the horizontal direction was -12.197 mm. The dynamic heat load induced by the beam can be significantly reduced from 0.54 to 0.22 W by adjusting the orbit of the beam at the horizontal direction from 12.197 to -7.367 mm. To meet the requirement of SR and long-time operation, the minimum dynamic heat load should be 0.14 W after beam commissioning and optimization.

The dynamic heat load was modest but larger than the theoretical calculation of that induced by image currents and SR. This may depend on the quality of the copper coating applied to the internal surfaces of the beam tube, which presented a higher resistivity than expected [20, 21]. Meanwhile, the temperature of the side flanges of the thermal shield, connected with the copper liner via flexible copper braids, reduced from 56.66 to 48.51 K when the orbit of the beam at the horizontal direction was adjusted from -12.197 to -7.367 mm (Fig. 14). The temperature of the copper liner increased due to the radiant and conductive heat of the beam tube, the temperature of which was increased by the image current, beam current loss, and SR.

The spectral characteristic parameters of the SR produced by the 3W1-SCW were tested. The characteristic energy of SR increased from 6.32 to 10.2 keV. The high-energy photon

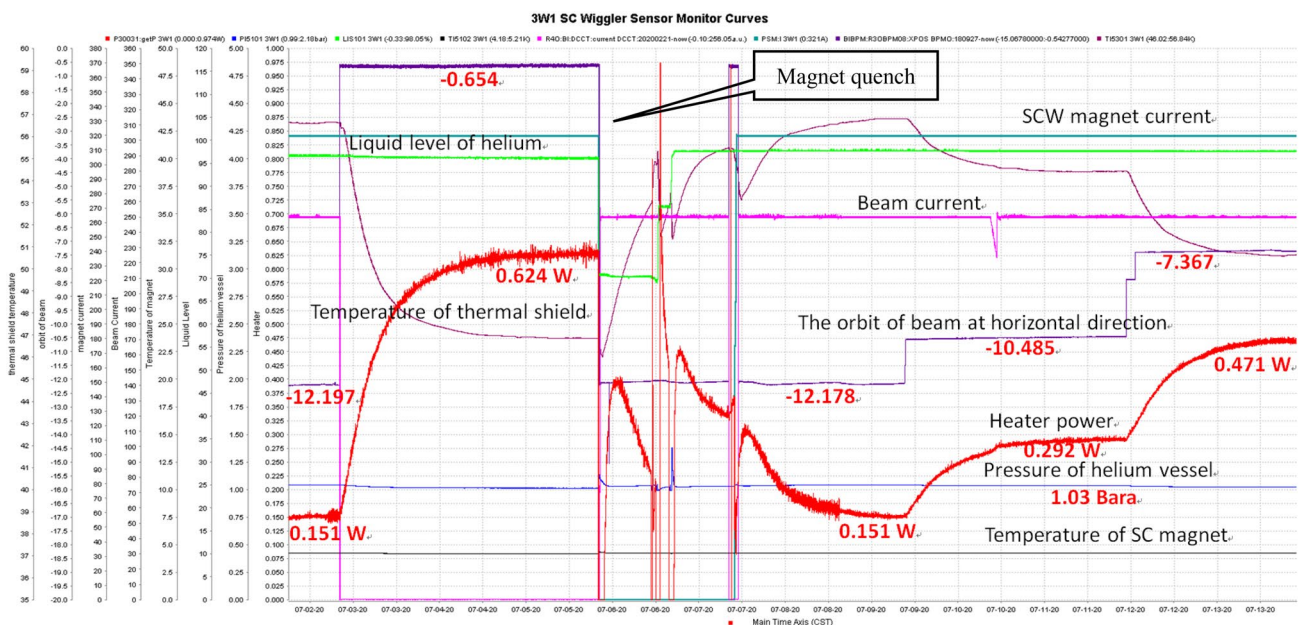


Fig. 14 (Color online) Measured dynamic heat load

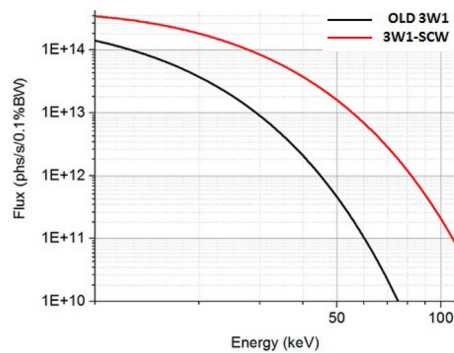


Fig. 15 (Color online) Test result of spectral characteristic

flux was 35 times higher at the photon energy of 50 keV (Fig. 15). Incorporating the 3W1-SCW in BEPC-II not only broadens the application field of the original 3W1 beamline station, but also greatly improves the use efficiency of the beamline.

9 Operation and quench

The 3W1-SCW has been operated for more than four months in the SR mode, and experienced cooling and rewarming five times. Magnet quenching occurred three times during the period of commissioning and normal operation. According to the calculation, there is approximately 100 kJ, which is 1/3 of the total stored energy of the magnet, should be taken away by the cryogenic system when quench. The liquid level of helium reduced from 95.91 to 70.39%, i.e., approximately 40 L of liquid helium evaporated in 2 s when the magnet was quenched. The pressure inside the liquid helium vessel increased rapidly, and the automatic pressure-relief valve opened instantly to discharge the pressure. The peak value of the pressure was 2.18 bara, which is lower than the set pressure of the 2nd safety valve. The level of liquid helium inside the helium vessel cannot meet the requirement of normal operation after magnet quench; therefore, it is necessary

to perform the liquid helium injection step, which would significantly affect the total system recovery time. Table 5 shows the magnet quench occurrence time, reason, and system recovery time of the 3W1-SCW. Figure 16 depicts the pressure of the helium vessel, the liquid level of the liquid helium, and the temperature of the magnet during magnet quenching.

10 Summary and conclusions

The 3W1-SCW cryostat was installed in a BEPC II storage ring and successfully operated with a beam in November, 2019. The static heat load of the 3W1-SCW was significantly reduced after structural optimization and improvement. The goal of zero liquid helium consumption was achieved, and the residual cooling capacity is approximately 0.69 W @4.2 K without the beam, equivalent to 12% of the total cooling capacity of a cryogenic system. A maximum magnetic field of 2.6 T was achieved and 2.49 T is acceptable for stored beam work; thus, 3W1-SCW has now been opened to the user community. The cryogenic system can operate stably when magnet quenching occurs three times, and has been running stably for more than four months. Cryostats with both liquid helium and cryocoolers have proven to be reliable and independent cryogenic systems for at least one maintenance cycle. The dynamic heat load induced by the beam can be reduced by adjusting its orbit. The characteristic energy of the SR increased from 6.32 to 10.2 keV. The high-energy photon flux increased 35 times at the photon energy of 50 keV. The developed 3W1-SCW not only expands the application fields of the old 3W1 beamline station, but also increases its efficiency. Operation of the 3W1-SCW demonstrates that the continuous operation of an SC device should cooperate with the beam dynamics.

Table 5 Magnet quench occurrence time, reason, and system recovery time of 3W1-SCW

Number	Occurrence time	Reason	System recovery time (h)
1	November 12, 2019	Magnet power supply volatility	36
2	July 5, 2020	Misoperation	21
3	September 25, 2020	City power supply volatility	20
Average time	25.67		

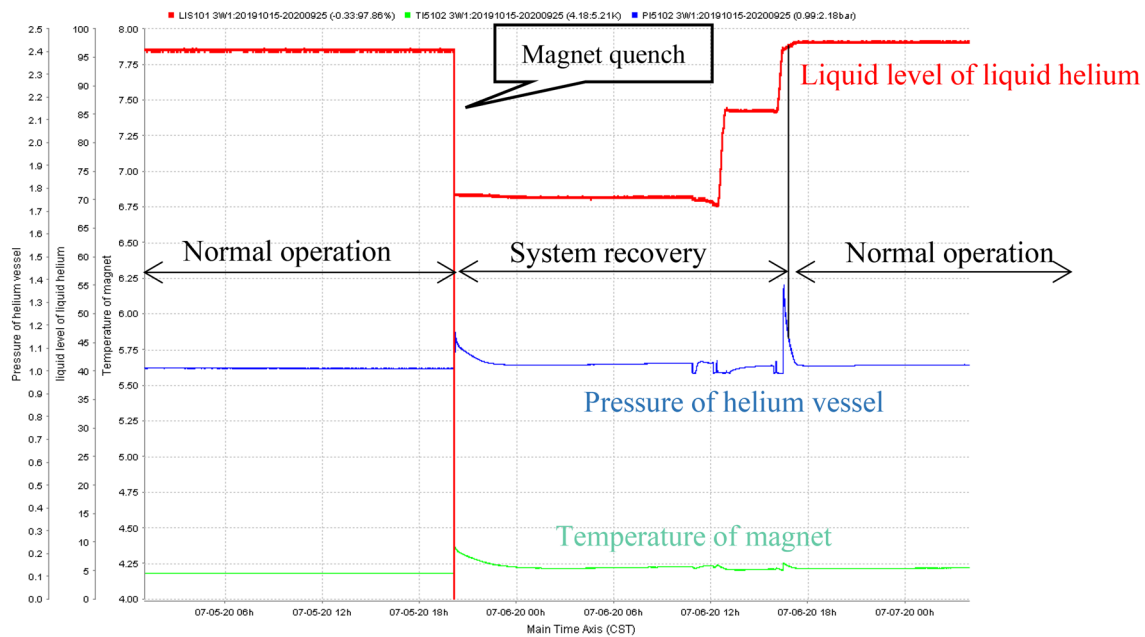


Fig. 16 (Color online) Pressure of helium vessel, liquid level of liquid helium, and temperature of magnet during magnet quench

Acknowledgements The authors thank Dr. C. L. Liu from the Institute of Plasma Physics, Chinese Academy of Sciences, for his technical support regarding the binary current lead. This work was supported in part by the High Energy Photon Source Test Facility and the Key Laboratory of Particle Acceleration Physics and Technology, Institute of High Energy Physics, Chinese Academy of Sciences.

Author contributions All authors contributed to the study conception and design. Material preparation, data collection and analysis were performed by Miao-Fu Xu, Xiang-Zhen Zhang, Rui Ye, Jin-Can Wang, Xiao-Juan Bian, Yao Gao, Min-Xian Li, Fu-San Chen, Xiao-Chen Yang and Rui Ge. The first draft of the manuscript was written by Miao-Fu Xu and all authors commented on previous versions of the manuscript. All authors read and approved the final manuscript.

Data availability The data that support the findings of this study are openly available in Science Data Bank at <https://doi.org/10.57760/sciencedb.08350> and <https://cstr.cn/31253.11.sciencedb.08350>.

Declarations

Conflict of interest The authors declare that they have no competing interests.

References

1. N.A. Mezentsev, E. Perevedentsev, Survey of superconducting insertion devices for light sources. Proceedings of the 2005 Particle Accelerator Conference, Knoxville, TN, USA, pp. 256–260. (2005) <https://doi.org/10.1109/PAC.2005.1590409>
2. A.A. Volkov, V.K. Lev, N.A. Mezentsev et al., Superconducting 119-pole wiggler with a 21-T field and 30-mm period length for the ALBA storage ring. *J. Surf. Investig.* **3**, 379–387 (2012). <https://doi.org/10.1134/S1027451012050199>
3. E. Wallén, G. LeBlanc, Cryogenic system of the MAX-Wiggler. *Cryogenics* **44**(12), 879–893 (2004). <https://doi.org/10.1016/j.cryogenics.2004.06.003>
4. E.C.M. Rial, J.C. Schouten, Electron beam heating effects in superconducting wigglers at Diamond Light Source. *IPAC'10*, 3195 (2010)
5. S. Khrushchev, V. Lev, N. Mezentsev et al. 3.5 Tesla 49-pole superconducting wiggler for DLS. *Proceeding of RuPAC*, 398 (2006)
6. N.A. Mezentsev, S.V. Khrushchev, V.K. Lev et al., Superconducting multipole wigglers: State of the art. *Proceedings IPAC*, (2014). <https://doi.org/10.18429/JACoW-IPAC2014-WEPR1091>
7. M.F. Xu, R. Ge, L. Bian et al., Design and research of cryostat for 3W1 superconducting wiggler magnet. *IEEE Trans. Appl. Supercond.* **28**(3), 1–6 (2018). <https://doi.org/10.1109/TASC.2018.2790380>
8. M.F. Xu, X.Z. Zhang, R. Ye et al., Design, assembly, and pre-commissioning of cryostat for 3W1 superconducting wiggler magnet. *Nucl. Sci. Tech.* **31**, 113 (2020). <https://doi.org/10.1007/s41365-020-00816-4>
9. X.Z. Zhang, M.F. Xu, R. Ye et al., Thermal analysis and experimental study of cryostat for superconducting wiggler of the HEPS-TF. *Cryogenics* **116**, 103307 (2021). <https://doi.org/10.1016/j.cryogenics.2021.103307>
10. N. Mezentsev, E. Wallén, Superconducting wigglers. *Synchrotron Radiat. News* **24**(3), 3–9 (2011). <https://doi.org/10.1080/08940886.2011.583883>
11. R.P. Reed, A.F. Clark, L.G. Rubin, *Materials at low temperatures*. Metals Park, Ohio 44073: American Society for Metals (1983). <https://doi.org/10.1063/1.2916172>
12. K.V. Zolotare, A.M. Batrakov, S.V. Khrushchev et al., High magnetic field superconducting magnets fabricated in Budker INP for Sr generation. *Proceedings of RuPAC XIX*, Dubna, 40–44 (2004)
13. A.A. Volkov, A.V. Zorin, V.Kh. Lev et al., The superconducting 15-Pole 7.5 Tesla wiggler in the LSU-CAMD storage ring. *Bull. Russ. Acad. Sci. Phys.* **79**, 53–59 (2015). <https://doi.org/10.3103/S1062873815010384>

14. M.N. Wilson, *Superconducting Magnets*. Oxford University Press (1983)
15. D. Bruno, W. Eng, P.K. Feng et al., RHC magnet electrical system. *Nucl. Instrum. Methods Phys. Res. A* **499**, 316–348 (2003). [https://doi.org/10.1016/S0168-9002\(02\)01941-1](https://doi.org/10.1016/S0168-9002(02)01941-1)
16. J.M. Nogiec, E. Desavouret, M. Lamm et al., Architecture of a software quench management system. In: *PACS2001 Proceedings of the 2001 Particle Accelerator Conference* (Cat. No.01CH37268), 5, 3460–3462 (2001) <https://doi.org/10.1109/PAC.2001.988144>
17. J.G. Weisend II. *Handbook of Cryogenic Engineering*. Taylor & Francis (1998)
18. M. Abe, Y. Murata, T. Seki et al., Magnetic field design of a superconducting wiggler in the SAGA-LS storage ring. *IEEE T. Appl. Superconduct.* **24**(2), 54–61 (2014). <https://doi.org/10.1109/TASC.2014.2304889>
19. T.W. Wysokinski, L.D. Chapman, D. Miller et al., 25+2 poles, 43 T wiggler at BMIT—7 years operational experience. *AIP Conf. Proc.* **1741**, 020026 (2016). <https://doi.org/10.1063/1.4952805>
20. C.C. Kuo, K.T. Hsu, G.H. Luo et al., Performance of the SRRC storage ring and wiggler commissioning. *Part. Accel. Conf. IEEE* **1**, 1582–1584 (1995). <https://doi.org/10.1109/PAC.1995.504726>
21. E. Wallén, G. Leblanc, T. Warwick, The MAX-wiggler: design, construction and commissioning of a 3.5 T superconducting wiggler with 47 poles. *AIP Conf. Proc.* **705**, 219–222 (2004). <https://doi.org/10.1063/1.1757773>

Springer Nature or its licensor (e.g. a society or other partner) holds exclusive rights to this article under a publishing agreement with the author(s) or other rightsholder(s); author self-archiving of the accepted manuscript version of this article is solely governed by the terms of such publishing agreement and applicable law.